IEEE TRANSACTIONS ON
MEDICAL ROBOTICS AND BIONICS

Design, Development, and Validation of a Self-Aligning Mechanism for High-Torque Powered Knee Exoskeletons

Sergei V. Sarkisian, Marshall K. Ishmael, Grace R. Hunt, and Tommaso Lenzi, *Member, IEEE*

***Abstract*— Powered knee exoskeletons aim to assist individuals with lower limb impairments by providing power and torque at the joint level. However, if the anatomical and exoskeleton joints are not perfectly aligned, the exoskeleton assistance may result in spurious forces and torques transferred to the user's limb. These spurious forces and torques can then generate undesired loads on the user's joint and shear stress on the user's skin, causing pain and ultimately undermining the exoskeleton assistance. To address this issue, we propose a novel powered knee exoskeleton with a self-aligning mechanism using a prismatic-revolute-revolute (PRR) configuration. The proposed self-aligning mechanism weighs 190 g (i.e., 5.3% of the total exoskeleton weight) and can transmit up to 120 Nm of torque at the knee joint (i.e., biological peak torque for a 50th percentile male climbing stairs). Our experiments show that during assisted sit-to-stand transfers the peaks of the spurious torques and forces are below 0.5 Nm and 5 N, respectively, even if misalignments are intentionally added between the user and the exoskeleton. This study supports the use of self-aligning mechanisms in powered exoskeletons.**

***Index Terms*— Human-robot misalignment, rehabilitation robotics, wearable robotics**

I. INTRODUCTION

POWERED exoskeletons have been proposed for rehabilitation [1], assistance [2]–[5], strength amplification [6], and productivity enhancement [7]. Regardless of the application, powered exoskeletons must transmit a controlled amount of torque to the wearer in a way that is safe, comfortable, and effective. Satisfying these objectives is particularly challenging due to the high variability of human anatomy. The measurements and proportions of the human body change significantly between users. In addition, the shape and volume of the human limbs depend on the muscle activation and the physical interaction with the exoskeleton [8]. As powered exoskeletons become more common, it is fundamental to understand how to design systems that can deal with this variability.

A fundamental challenge arising from the variability of the human anatomy consists of aligning the rotational axis of the powered exoskeleton joint with the axis of the anatomical joint of the user [8]. Anatomical joints, such as the knee show both rolling and sliding motions, which result in a non-constant, moving axis of rotation [9]. Even if these sliding movements are neglected, perfect static alignment between the powered and anatomical axes is not possible as the anatomical axis cannot be located accurately when wearing the powered exoskeleton. Finally, a perfectly aligned exoskeleton may become misaligned due to the compression of the user's soft tissues or flexibility of the human-robot interface generated by the interaction forces between the user and the exoskeleton [8].

Regardless of the cause, misalignments may result in spurious forces and torques applied to the user [10], [11]. In turn, these spurious forces and torques may produce unwanted load on the user's joint and shear stress on the user's skin, which reduces comfort and may even be unsafe for the user [8]. To address this issue, researchers have proposed adding passive degrees of freedom (pDOF) to the human-robot kinematic chain [12]. Theoretical studies show that this strategy can enable the powered exoskeleton joint to passively follow the anatomical joint movements [10], [13]. These pDOFs have been commonly referred to as self-aligning mechanisms.

Several self-aligning mechanisms have been proposed. Saccares *et al*. have presented a self-aligning powered knee exoskeleton with 5 pDOFs including two connected four-bar linkages for power transmission [5] Cai *et al.* have shown a self-aligning exoskeleton for knee assistance with 6-DOF kinematic chain configuration [14]. In [15], Celebi *et al.* have proposed a self-aligning knee exoskeleton with Schmidt coupling—a 3-DOF mechanism accommodating translational motion of the knee joint center of rotation in the sagittal plane and a rotary joint for knee flexion/extension. Junius *et al*. have performed a range of motion (ROM) and pDOF displacement validation using motion capture on a passive self-aligning hip orthosis with 3 pDOFs equivalent to the anatomical hip joint [16]. The same group has investigated the effects of a self-aligning mechanism on metabolic consumption and muscle activation [17]. Giovacchini *et al.* have presented a powered hip orthosis with 3 lockable pDOFs designed to adjust the exoskeleton size to different users [18]. Lee *et al.* have presented the design of a flexible leg exoskeleton with a three-pulley system for misalignment compensation at the knee. In [19], Ergin *et al.* have shown a self-aligning mechanism for a powered knee exoskeleton with 3 pDOFs in RRP configuration. A polycentric mechanism imitating the physiological movement of the anatomical knee joint has been presented in [20]. Although several powered exoskeletons with

Manuscript submitted for review on 10/09/2019. This work was partly supported in part by the National Institute for Occupational Safety and Health under Grant T42/CCT810426 and the US Department of Defense under Grant W81XWH-16-1-0701.

S. V. Sarkisian, M. K. Ishmael, G. R. Hunt, and T. Lenzi are with the Department of Mechanical Engineering and the Utah Robotics Center at the University of Utah, Salt Lake City, UT, 84112, USA. (e-mail: sergei.sarkisian@utah.edu)

Digital Object Identifier: 10.1109/TMRB.2020.2981951

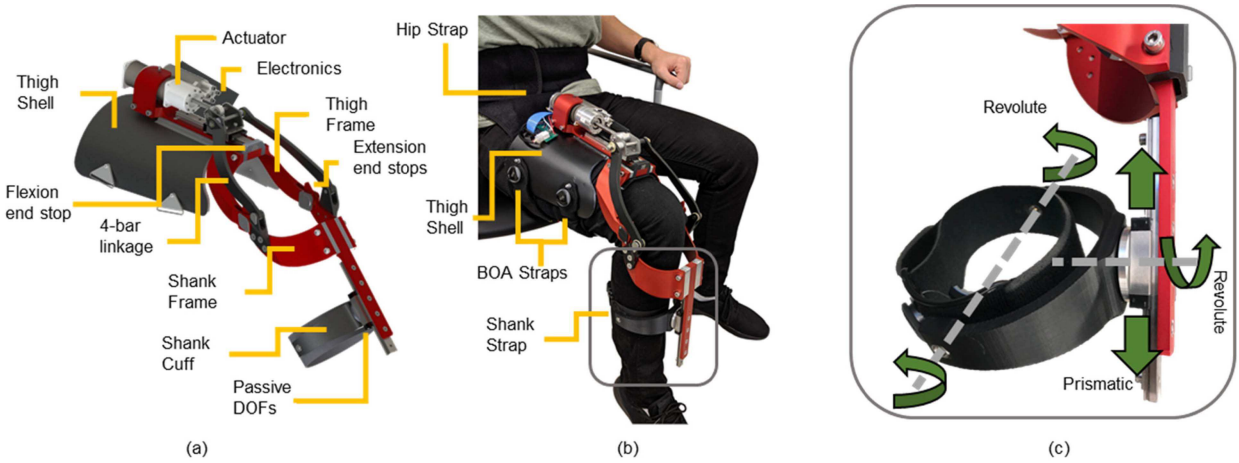

Fig. 1. (a) CAD model of Utah ExoKnee with major components labeled. (b) User wearing Utah ExoKnee. A hip strap wraps around the user's waist and thigh. The exoskeleton is attached to this hip strap by Velcro that covers the inside of the thigh shell. The exoskeleton is tightened around the thigh using BOA®straps. (c) Zoomed in view of Utah ExoKnee self-aligning mechanism. Three pDOFs are used in PRR configuration.

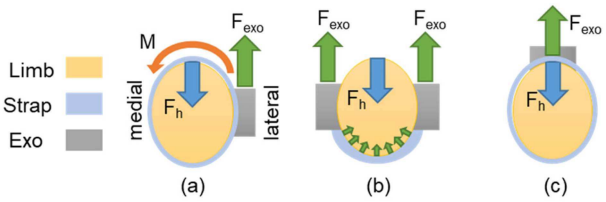

Fig. 2. Schematic diagram of three different ways of attaching exoskeletons to a user's limb. F_{exo} is the force applied by the exoskeleton and F_h is the reaction force of the human limb. In (a), M is the torsional moment created by the F_{exo} and F_h couple. Utah ExoKnee uses the attachment configuration shown in (b) at the shank, where the force is transmitted to the limb through a soft flexible strap attached to the frame on both sides, the attachment configuration shown in (c) at the thigh, where the force is transmitted through a soft flexible strap attached to a frame on the front of the limb.

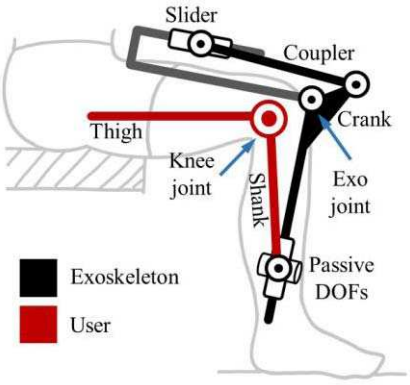

Fig. 3. Kinematic scheme of the Utah ExoKnee worn by a user. The human leg and the exoskeleton form a closed kinematic chain, allowing movement between the exoskeleton and the user's shank.

self-aligning mechanisms have been previously developed, validation is still lacking, as no study has directly assessed the spurious forces and torques on human users during assistive tasks that require high torque such as sit-to-stand transfers.

In this paper, we present the design, development, and validation of a powered knee exoskeleton, namely Utah ExoKnee, with a self-alignment mechanism. Utah ExoKnee is designed to assist with tasks that required high assistive torque, such as climbing stairs and performing sit-to-stand transfers. The proposed self-aligning mechanism comprises three pDOFs in prismatic-revolute-revolute (PRR) configuration connecting the human leg to the exoskeleton actuated joint. We hypothesize that, with the proposed knee exoskeleton, misalignments between the user and the robot rotation axes will not result in an increase of spurious forces and torques on the user. This hypothesis shall be tested by measuring the physical interaction between able-bodied users and the proposed knee exoskeleton during the execution of assisted sit-to-stand transitions while controlled misalignments are introduced by the experimenter.

II. Design

A. Frame and Physical Human Robot Interface

Utah ExoKnee is designed to minimize spurious forces and torques on the user's leg. In contrast to the common lateral location shown in Fig. 2(a), the proposed exoskeleton frame is located on the top of the leg, using the design configurations shown in Fig. 2(b) for the shank segment and in Fig. 2(c) for the thigh segment. In this symmetric design configuration, the assistive exoskeleton force (F_{exo}) intersects the limb central axis. Thus, it generates no torsional moment (M), which provides a key advantage for the design. On one hand, there is not torsion on the user's limb. Thus, there is no shear stress on the user's skin, which may cause discomfort and even pain [21]. On the other hand, there is no torsion on the exoskeleton frame at the point of contact with the user. Thus, this configuration helps the self-aligning mechanism to avoid torsion, which may result in binding of the mechanism and, generally, would require heavier and bulkier structures.

To locate the exoskeleton actuation on top of the thigh (anterior surface of the thigh), the exoskeleton frame must wrap around the leg without interfering with it, which somewhat

TABLE I
UTAH EXOKNEE WEIGHT BREAKDOWN

Component	Mass (kg)	Subcomponent	Mass (kg)
Exoskeleton	2.5	Frame	1.525
		pDOFs	0.190
		Actuator	0.785
Electronics pack	1.1	Battery	0.320
		Electronics	0.780

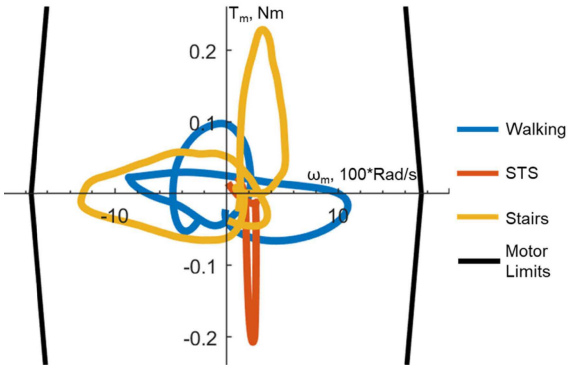

Fig. 4. Simulated motor performance during level ground walking (blue), sit-to-stand transitions (orange), and stairs ascent (yellow). The X-axis shows the motor speed in rad/s divided by 100 for visual clarity. Y-axis shows the motor torque in Nm. Motor's stall torque is 3.22 Nm and the no-load speed is 1750 rad/s (∼16700 RPM).

increases the design complexity. Each segment of the exoskeleton frame comprises two symmetrical halves wrapping around the user's limb and machined from 7075 aluminum alloy (420g thigh side, 256g shank side). These halves are designed to fit a 50th percentile male adult, which resulted in 160 mm and 115 mm diameter of the thigh and shank segment, respectively. The distance between the knee joint hinges of the exoskeleton frame in the frontal plane can be increased to accommodate larger users through the insertion of spacers. The thigh and shank segments are connected to form the exoskeleton knee rotational joint, using steel shafts and low-friction plastic bushings (Inglide Z, IGUS, Germany). Two extension end stops are integrated into the exoskeleton shank and thigh frames to prevent the exoskeleton knee joint from hyperextending (Fig. 1(a)). The flexion end stop is integrated into the thigh frame and limits the range of motion of the linear guide carriage, resulting in 100^{o} maximum flexion knee angle.

The thigh segment of the exoskeleton connects to the wearer's thigh through a flexible plastic molded thigh shell, the inner surface of which is lined with Velcro (Fig. 1(a)). The user wears a hip strap wrapping around his/her waist and thigh. The Velcro on the inner side of the thigh shell connects to the thigh portion of the strap (Fig. 1(b)), improving the physical connection between the exoskeleton and the user. The shell is tightened around the thigh using BOA®system straps with magnetic buckles for quick donning (Fig. 1(b)). The thigh shell is flexible, allowing users with different thigh sizes/shapes to use the exoskeleton comfortably. The shank segment uses a C-shaped frame with an adjustable strap to adapt to different users and tighten the strap securely to the limb (Fig. 1(a)).

Utah ExoKnee uses a self-aligning mechanism with three pDOFs. As shown in Fig. 1(c), the three pDOFs are arranged in prismatic-revolute-revolute (PRR) configuration and integrated in series with one active revolute DOF (knee flexion/extension). The prismatic pDOF is achieved using a low-friction linear guide (150 g, 75-mm range of motion (ROM), SSELBZ13, Misumi, Japan) connected to the lower link of the exoskeleton (i.e., shank segment). The linear guide carriage is attached to a custom rotary joint (25 g, Table I), which is a multi-turn joint with no mechanical stop. In turn, this custom rotational joint holds a C-shaped, 3D printed frame, which connects to a flexible cuff through a perpendicular rotary DOF (15 g, Table I). A video of the Utah ExoKnee showing the active and passive degrees of freedom is available in the supplementary material.

TABLE II
UTAH EXOKNEE PERFORMANCE METRICS

Rated power output	170 W
Peak torque	120 Nm
Max speed	4.5 rad/s

B. Transmission and Actuation

Utah ExoKnee is designed to provide the knee torque and speed required by a 50th percentile male adult to climb stairs and walk on level ground. From the analysis of able-bodied biomechanics [22], we can see that satisfying this design objective results in peak torque of 120 Nm (in stair descent) and a peak angular speed of 4.5 rad/s (257^{o}/s, 105 steps/min in level-ground walking). Utah ExoKnee satisfies these requirements using a four-bar mechanism in offset slider-crank configuration powered by a linear actuator. The slider joint is designed to travel along the thigh and on top of it as shown in Fig. 1. The location of the slider imposes a constraint on the offset of the four-bar mechanism with respect to the exoskeleton knee joint position, which was chosen to be 103 mm based on 50th percentile male thigh dimensions. Starting from this offset value, the dimensions of the crank and connecting linkages forming the four-bar mechanism (II) were selected using the iterative design process described in [23]. This design process accounts for both the dimensional constraints imposed by the user's leg, the torque and speed demands obtained from biomechanics studies, and the torque, speed, and thermal constraints due to the electromechanical actuator. Forces and ROM for each component of the four-bar mechanism are computed in simulations and used to drive the mechanical design.

A reaction force sensing series elastic actuator (RFSEA) (Orion P-170, Apptronik, USA) powers the slider joint as shown in Fig. 1(a) [24]. RFSEAs differ from the more common force sensing series elastic actuators because the elastic element is placed between the motor and the frame, rather than between the motor and the output joint. The actuator

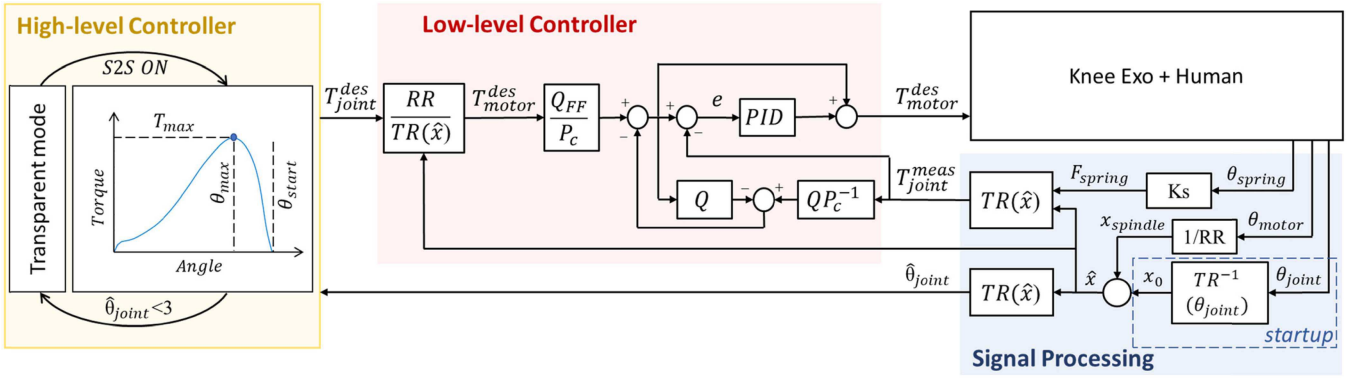

Fig. 5. Block diagram of the control and signal processing systems. All variables are defined and described below, in section D, Signal Processing and Control. At the high-level, a controller based on a finite-state machine defines the desired knee torque. At the low-level, a closed-loop torque controller with disturbance observer defines the desired motor current that is then imposed using a current driver. Raw signals are processed in the embedded electronics to estimate the angular position and torque at the knee joint.

uses a ball screw system (8×2 mm, custom machined from a stock ball screw) where the nut is driven by a timing belt and supported by two angular contact bearings. The belt pulley system has a 2.5:1 transmission ratio and is connected to a brushless DC motor (EC 4-Pole 30 200W, Maxon Motors, Switzerland). The actuator features a sliding element that acts as a bridge between the actuation system and the ground. This sliding element anchors directly to the exoskeleton thigh frame and is connected to the actuation part through two identical pre-compressed coil springs. The ball screw is supported by a low-friction linear guide (SSELBZ13, Misumi, Japan) that prevents radial loading on the ball screw. The actuator combined with the exoskeleton frame and human-robot interface extends by approximately 70 mm on top of the thigh. The RFSEA in combination with the proposed four-bar mechanism enables Utah ExoKnee to satisfy the torque and speed objective (120 Nm, 257 deg/s) while fitting the anthropometry of the 50th percentile adult male without hardware modifications. The exoskeleton performance metrics are summarized in Table II.

C. Sensors and Embedded Electronics

Utah ExoKnee comprises an array of sensors to accurately control the human-robot interaction. An absolute magnetic rotary encoder (RM08 SD, RLS, Slovenia) placed on the actuated joint of the exoskeleton estimates the absolute knee joint position. An incremental magnetic rotary encoder (RM08 SD, RLS, Slovenia) located on the motor shaft measures its position and is used to estimate motor angular velocity. In addition, the RFSEA is equipped with a high-resolution rotary absolute encoder (Vert-X 1302, Contelec, Switzerland) that measures the deflection of the linear springs using a capstan coupling. The capstan coupling converts the linear displacement due to the deflection of the springs into a proportional angular displacement of the encoder shaft, which is driven by a steel cable [24]. For the goal of this experiment, a 6-axis load cell (M3713D, Sunrise Instruments, China) is integrated into the exoskeleton shank segment to accurately measure the physical interaction between the user and the robot as necessary to assess the function of the self-aligning mechanism. The 6-axis load cell uses an off-the-shelf signal amplifier and a custom acquisition board (AD7609, Analog Devices, USA). The force and torque recordings from the 6-axis load cell are synchronized with the exoskeleton controller using a digital signal.

The exoskeleton is controlled using a custom embedded system including two different processing units that run the control routines and the secondary functions such as data logging and Wi-Fi communications. All time-critical routines such as sensor reading, filtering, joint position and torque control loops, run at 2 kHz on a 32-bit microprocessor (Atmel MK20DX256). The microprocessor communicates with the motor current servo controller (Elmo Motion Control, G-TWI10/100SE) using PWM. The high-level control loops, data-logging, and user-communication run on a single-board computer (Raspberry-Pi, Model 3A+) at 500 Hz. The single-board computer communicates with the microprocessor using SPI. An external laptop runs a custom GUI for data monitoring and parameter-selection purposes and communicates via using Wi-Fi with the single-board computer. The GUI is used to change the control parameters and start/stop data saving. In addition, the control system uses a 1050 mAh 6-cell lithium-polymer battery, and a 5-V regulator to power the processing units, embedded sensors, and current servo controller. The electrical power consumption is 3.8 W and 3.1 W with Wi-Fi on and off, respectively. The weight of the embedded electrical system, including battery and protective covers, is 1.1 kg.

D. Signal Processing and Control

A block diagram of the sensor processing is shown in Fig. 5. At startup, the absolute encoder (θ_{joint}) estimates the absolute position of the slider (x_0) using the inverted four-bar kinematics ($TR^{-1}(\theta_{joint})$). The absolute position of the slider is then used in combination with a relative slider position ($x_{spindle}$) estimated from the motor encoder (θ_{motor}), to obtain an accurate (+/− 0.011 mm) measurement of the slider position ($\hat{x}$). The slider position is used to calculate the position-dependent transmission ratio of the four-bar kinematics ($TR(\hat{x})$). Similarly, the knee joint torque

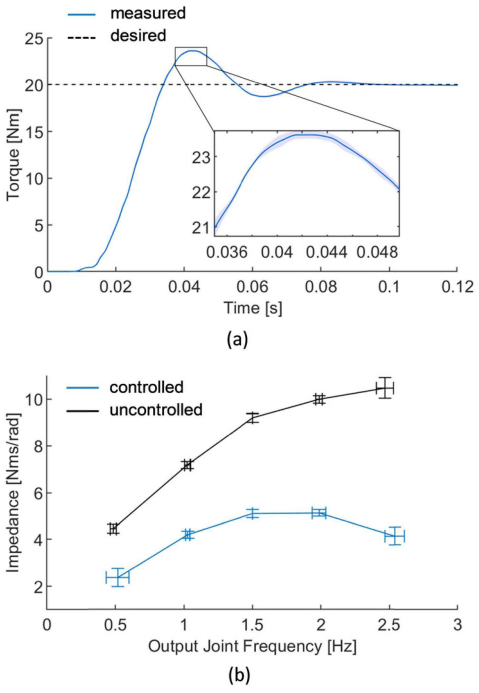

Fig. 6. Torque step response (a) and output impedance (b) of the knee exoskeleton under the proposed closed-loop control. The controlled and uncontrolled system dynamics are shown with black and blue lines, respectively. Horizontal bars represent the standard deviations of the joint velocity. Vertical bars show the standard deviations of the estimated output impedance.

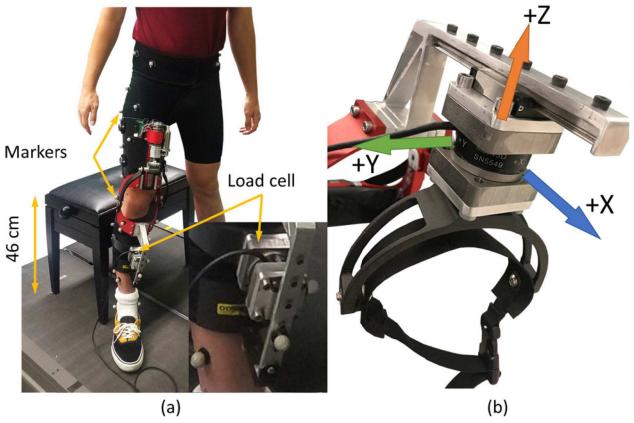

Fig. 7. Experimental setup during testing of Utah ExoKnee (a). Markers were placed on subjects' pelvis, thigh, shank, and ankle. Markers were also placed on the exoskeleton's thigh and shank parts. An additional marker was placed to track the movement of the prismatic pDOF. In (b) the positioning and orientation of the load cell is shown. The load cell was added during experimentation and is not a permanent part of Utah ExoKnee.

(T^{meas}_{joint}) is estimated using the spring force (F_{spring}) combined with transmission ratio $(TR(\hat{x}))$. The spring force (F_{spring}) is estimated by measuring the spring deflection (θ_{spring}) in combination with the stiffness of the springs (Ks) and the transmission ratio $(TR(\hat{x}))$.

At the low-level, a closed-loop controller is implemented after [24] [25] to accurately track the desired knee-space torque (T^{des}_{joint}). First, the desired knee-space torque (T^{des}_{joint})

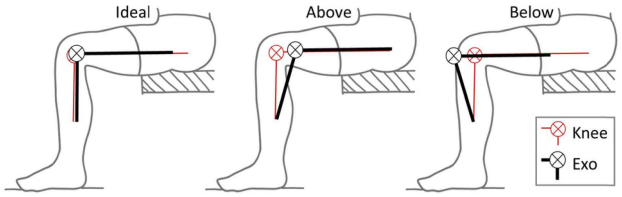

Fig. 8. Three alignment conditions used during the experiment. Each subject was fitted with the exoskeleton in Ideal, Above, and Below alignment. The Ideal condition was set up by the experimenter visually aligning the exoskeleton and anatomical knee axes. Using a measuring tool, a misalignment of approximately 25 mm between the knee and the exoskeleton joints was introduced in both Above and Below conditions.

is transformed into an equivalent desired motor-space torque (T^{des}_{motor}) using the four-bar transmission ratio $(TR(\hat{x}))$ and the combined timing-belt/ball screw transmission ratio (RR). The desired motor torque is then fed to a closed-loop proportional-integral-derivative (PID) regulator with disturbance observer (DOB). As proposed in [24], the RFSEA is modeled as a second-order system (P_c) as follows.

$$P_c(s) = \frac{800000}{84.98s^2 + 4674s + 800000} \tag{1}$$

Exogenous forces and torques are handled as disturbances and fed as inputs to the system to compensate for the observed torques not resulting from the modeled system using feed-forward (Q_{FF}) and feedback filters (Q). Finally, the desired motor torque (T^{des}_{motor}) is transmitted to the off-the-shelf current driver on the knee exoskeleton.

At the high-level, a torque-angle relationship based on healthy biomechanics defines the desired knee torque (T^{des}_{joint}) during sit-to-stand transitions solely as a function of the knee joint position $(\hat{\theta}_{joint})$, similar to the stair-ascent controller described in [26]. As can be seen in Fig. 5, the desired knee torque starts at zero when the subject is seated, and the knee joint is flexed. As the user stands-up, the exoskeleton knee joint starts extending from its resting position. As a result, the desired exoskeleton torque increases from zero to a maximum value (T_{max}). From its maximum, the torque decreases with the knee joint position, finally reaching zero when the knee joint is fully extended. Notably, the user's knee angle at the start of the sit-to-stand transition depends on the user's anthropometry, chair height, and posture. To accommodate this variability, the knee angle at which the exoskeleton starts providing torque (θ_{start}) equals the measured knee angle when the sit-to-stand controller is activated. Moreover, the desired peak torque (T_{max}) can be adjusted by the experimenter through a GUI. The knee angle at which the peak torque is achieved (θ_{max}) happens at 30% between the starting and the ending angle. The torque-angle relationship is implemented with a parametric Look-Up Table (LUT) after [27]. For the goal of this experiment, the sit-to-stand mode is activated by the experimenter through a graphical user interface (GUI) using a push-button $(S2S\ ON)$. Once the knee angle reaches 3° the standing-up task is considered completed, and the controller automatically switches to a transparent mode, where interaction torque is minimized by closed-loop control.

III. Bench-Top Testing

A. Experimental Methods

Benchtop characterization was performed to evaluate the performance of the closed-loop torque controller. During a first test, the exoskeleton was constrained on the benchtop to prevent movements of the joint. Then, a closed-loop PID system was tuned experimentally using the step-input response to obtain a rise time of less than 20 ms, a settling time of less than 70 ms, and less than 20% overshoot. After tuning was completed, a torque chirp input with 8 Nm amplitude and frequency ranging from 0.1 to 20 Hz was applied to the system while the output torque was recorded. The result of the chirp test was used to obtain an accurate dynamic model of the closed-loop system (P_n), which is necessary for the DOB (see Fig. 5). The model was identified using the System Identification Toolbox (MATLAB, MathWorks, USA). After the identified model was applied to the DOB, we imposed a 20 Nm torque step input for ten consecutive times. The 20 Nm step was the maximum value our bench top setup could withstand. A second test was performed to assess the output impedance of the closed-loop system. For this test, we removed the physical constraints on the output joint and command 0 Nm at the joint. Then, we recorded the measured joint torque while manually back driving the joint. To this end, an experimenter moved the output joint in correspondence with visual and auditory cues that mimicked that of sine waves ranging from 0.5 Hz to 2.5 Hz with 0.5 Hz intervals. The measured joint torque and joint velocity were then used to estimate the output impedance ($Z = T(f)/\dot{\theta}(f)$) as a function of the output joint frequency (f). Discrete Fast Fourier Transform was applied to the time-domain signals recorded during each test separately. Then, we computed the torque-to-speed ratios representing the output impedance. The standard deviation of both the impedance estimate and input frequency is shown in II-D as a measure of the test variability. The test was performed with the control on and off to estimate the controlled and uncontrolled system dynamics, respectively.

B. Experimental Results

The results of the torque step response for the proposed closed-loop system are shown in II-D(a). The rise time was 15.2 ms. The settling time was 69.2 ms. The overshoot was 17.5% (3.5 Nm). The steady-state error was 0.001 Nm. Based on the rise time and using a second-order model, the -3dB bandwidth of the closed-loop system is estimated to be 22.3 Hz. The results of the impedance test are shown in II-D(b). The output impedance has a peak of 5.14 Nms/rad at 1.98 $\pm$ 0.05 Hz. On average, the output impedance was 49.2% lower for the controlled system than the uncontrolled system.

IV. Human Experiments

A. Experimental Protocol

The performance of Utah Knee Exoskeleton was tested on four young healthy subjects (three male, one female; 25.5$\pm$1.12 years old, 178$\pm$9.52 cm, and 72.3$\pm$7.95 kg). All subjects were given 30 minutes a day for two days to familiarize themselves with the exoskeleton prior to the experiments. Subjects were asked to stand up from a bench (46-cm tall) with their arms crossed while wearing the powered knee exoskeleton. The displacement of the exoskeleton relative to the subject's limb and the interaction forces and torques were the main experimental outcomes. The experimental protocol was approved by the University of Utah Institutional Review Board. Written informed consent was provided by the subject before the experiment took place. The subjects consented to disseminate pictures and videos of the experiments.

The physical interaction between the subject and the exoskeleton was measured using a 6-axis load cell (M3713D, Sunrise Instruments, China). The load cell was placed between the linear guide carriage and the exoskeleton shank segment as can be seen in Fig. 7. The data from the load cell were acquired at 500 Hz using a National Instruments MyRIO controller which was synchronized on-line with the exoskeleton's controller. The exoskeleton's embedded electronics recorded the output of all onboard sensors, including the angular position of the knee joint and the applied knee torque. A motion tracking system (Vicon Motion Systems Ltd., United Kingdom) was used to measure the motion of the subject's thigh and shank, and the motion of the exoskeleton, including its pDOFs. For this experiment, the marker set shown in Fig. 7 was used to track the knee joint angle, the exoskeleton joint angle, the movement of the exoskeleton relative to the subject's limb, and the displacement of the pDOFs.

Motion capture data was post-processed using Vicon Nexus (Vicon Motion Systems Ltd., United Kingdom). The functional axis of the knee was calculated in Vicon Nexus using the symmetrical axis of rotation approach (SARA) [28]. Visual 3D (C-Motion, USA) was used to filter the trajectory data (6^{th} order bidirectional 6Hz Butterworth filter), extract the joint angles of the exoskeleton and subject's knee, and calculate the movement of the exoskeleton's pDOFs. The beginning and end of each sit-to-stand period were found by identifying the local minima and maxima of the subject's knee angle. MATLAB (MathWorks, USA) was used for all further post-processing. The kinematic data were synchronized with the signals from the exoskeleton and the load cell controllers. Each sit-to-stand was then segmented using the frame numbers of the beginning and end of each sit to stand period and normalized to 1000 samples.

We evaluated the effect of misalignment between the exoskeleton joint and the anatomical joint at different assistance levels. Each subject tested nine experimental conditions. Specifically, we imposed three different alignment conditions and three levels of assistive torque. The three alignment conditions were imposed by aligning the exoskeleton knee joint in three positions: 1) *Ideal* positioning at the level of the anatomical knee joint, 2) *Above* the anatomical knee joint by approximately 25 mm, and 3) *Below* the anatomical knee joint by approximately 25 mm. Each alignment was tested at each of three levels of assistance: 1) *Zero* desired torque, 2) *Low* assistive torque of approximately 25 Nm at the peak, and 3) *High* assistive torque of approximately 50 Nm at the peak. For each of these nine conditions, each participant was asked

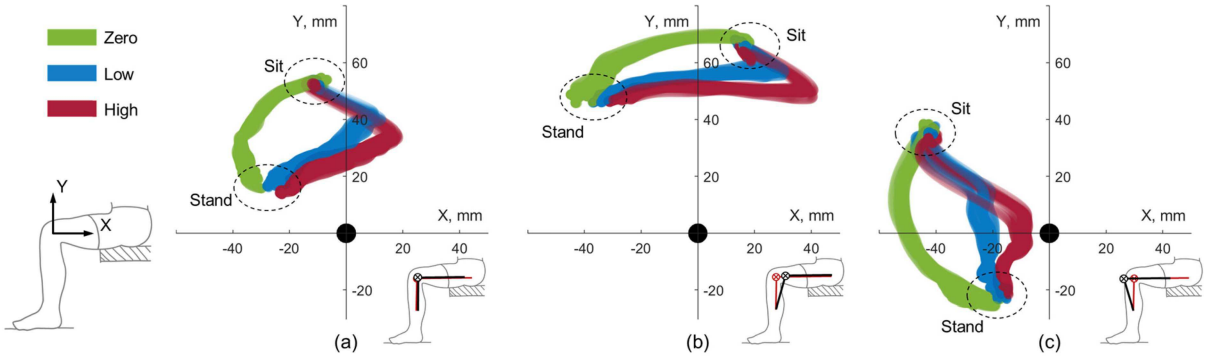

Fig. 9. Position of the exoskeleton's axis relative to the subject's knee joint axis in the Sagittal plane during the sit-to-stand movements (i.e., no stand-to-sit movement). Ideal alignment case is shown in panel (a), the Above case is shown in panel (b), and the Below case is shown in panel (c). Results from zero, low, and high assistance levels are shown in each panel using green, blue, and red, respectively. In all panels, the origin of the coordinate axes indicates the position of the subject's knee joint axis. Thus, a value closer to zero means that the exoskeleton joint axis is closer to the subject's knee joint axis.

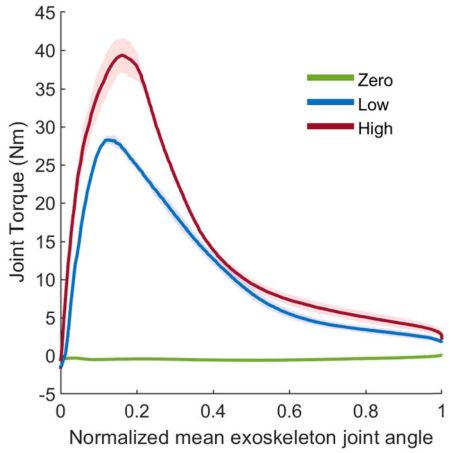

Fig. 10. Desired torque profile applied during sit-to-stand testing, averaged across all trials and subjects. Three assistance levels are shown: Zero torque, Low assistance level, and High assistance level. The X-axis represents normalized knee angle from initial to final angle during sit-to-stand.

to stand up from a seated position 10 times. Our working hypothesis is that the misaligned conditions will result in a greater movement of the pDOFs, and that the higher assistive levels will result in greater misalignments, but that neither will result in greater spurious forces and torques. A video of a subject performing the experimental protocol is available in the supplementary material.

B. Experimental Results

The position of the exoskeleton joint axis relative to the subject's knee axis is shown in Fig. 9, where the origin of the coordinate axes indicates the position of the subject's knee joint axis. As can be seen in Fig. 9, the position of the exoskeleton joint axis during the sit-to-stand transition was not fixed but followed a different profile depending on the alignment and the assistance level conditions. Specifically, as shown in panels (a), (b), and (c) of Fig. 9, changing the alignment condition of the exoskeleton, resulted in a rotation of the position profile about the subject knee angle. The *Above* condition (b) resulted in displacements that form an arc superior to the subject knee joint, and the *Below* condition (c) resulted in displacements that form an arc anterior to the subject knee joint. Moreover, changing the assistance level as shown with different colors in Fig. 9, affected the shape of the position profiles. In all *Zero* assistance conditions, the position profile forms an arc that curves away from the subject knee, roughly maintaining the same absolute displacement from the subject knee axis while rotating about it. In contrast, the *Low* and *High* assistance conditions resulted in position profiles that are closer to the subject knee axis during the middle of sit-to-stand transition reversing the concavity of the displacement arc observed for *Zero* condition. Notably, for each alignment conditions, at the start and end of the sit-to-stand transitions, when the assistive torque is zero, the positions observed for different assistive conditions seem to match. Thus, the position of the exoskeleton joint axis relative to the subject's knee axis is not fixed but changes during sit-to-stand transitions as a function of both the alignment and the assistance conditions.

The reaction forces and torques measured by the 6-axis load cell are shown in Fig. 11 as a function of the normalized sit-to-stand transition time. The average values for the measured reaction forces across all experimental conditions ranged between -0.769 N and 0.844 N for F_x, 4.99 N and 11.8 N for F_y, -1.44 N and 51.9 N for F_z, -1.07 Nm and 0.808 Nm for T_x, -0.129 Nm and 0.315 Nm for T_y, 0.0629 Nm and 0.110 Nm for T_z respectively. As can be seen in Fig. 11, F_z, which is approximately perpendicular to the subject's shank, had a large peak during the middle of a sit-to-stand transition in *Low* and *High* assistance conditions and stayed near zero during the *Zero* assistance condition when no torque is applied by the exoskeleton. This behavior did not change across alignment conditions. In contrast, F_x, T_y, and T_z displayed no systematic changes during sit-to-stand, or across alignment or assistance conditions. F_y and T_x trended slightly upward and downward, respectively, from the beginning of sit-to-stand to the end. However, this behavior showed no systematic changes across alignment or assistance conditions.

A linear regression analysis was conducted to assess the potential correlation between the interaction forces and torques measured by the load cell and the torque applied by the

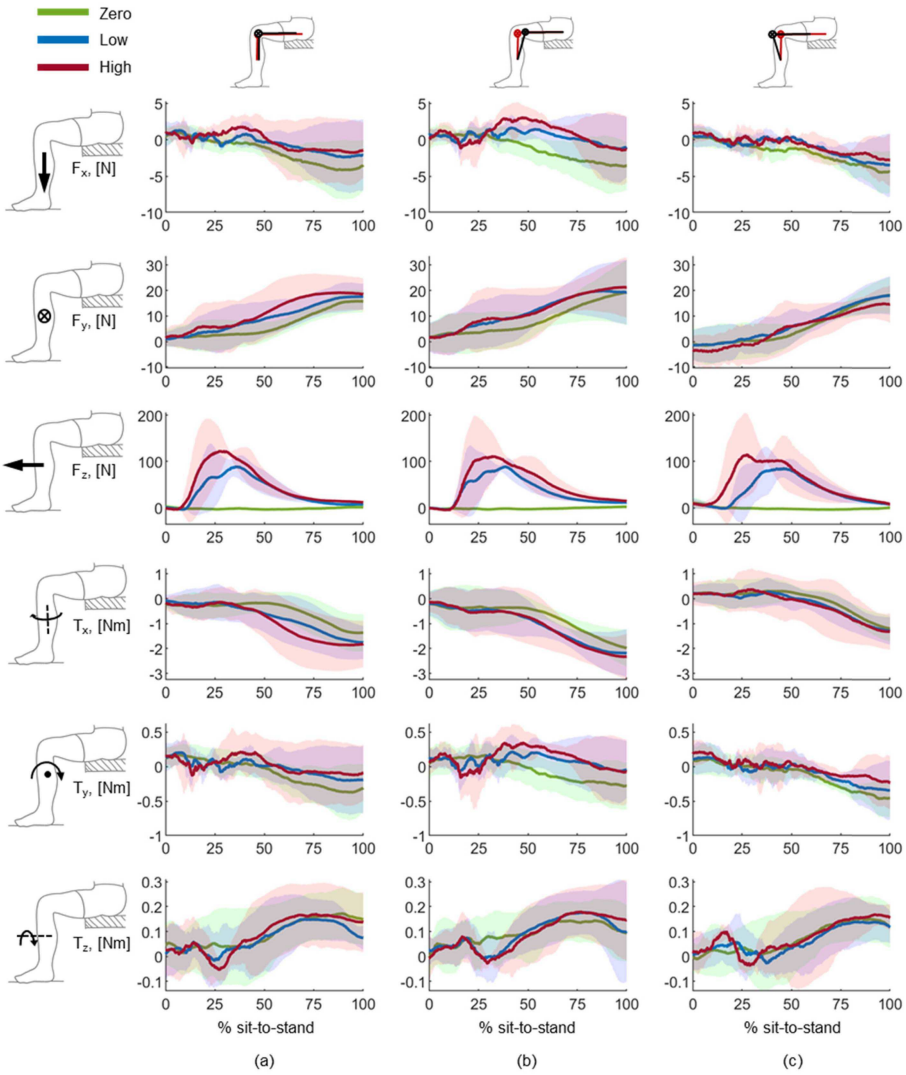

Fig. 11. Mean values (solid lines) and standard deviations (shaded areas) of the interaction forces and torques between the subjects' shank and exoskeleton. Ideal alignment case is shown in (a), Above case is shown in (b), and Below case is shown in (c). On the plots only the sit-to-stand movements are shown (no stand-to-sit movement). The assistance levels are indicated with different colors: zero assistance in green, low assistance in blue, and high assistance in red.

exoskeleton R^2 values above 0.98 were found between joint torque and F_z in low assistance and high assistance conditions, across all alignment conditions. In contrast, the average R^2 values for F_x, T_y, and T_z across all conditions were 0.133, 0.0643, and 0.155, respectively. This analysis suggests a highly significant correlation between the applied torque and the F_z, and no correlation with the other measured interaction forces and torques.

The mean and standard deviations of knee angles and the movement of each pDOF for each tested condition are shown in Fig. 12. The knee angle was not noticeably impacted by changes in alignment or assistance. All three pDOFs showed systematic changes with changing assistance levels, and there were some changes in displacement profiles when the alignment was changed (IV-B). The sagittal pDOF displacement increased with increasing assistance. In low and high assistance conditions, a peak displacement was observed at approximately 30% of sit-to-stand. The *Above* alignment condition exhibited both the largest peak displacement and the largest range of displacement from beginning to end of sit-to-stand. The *Below* alignment condition showed the least change from beginning to the end of sit-to-stand. The frontal pDOF also increased systematically with increasing assistance, and the shape of the displacement profile in low and high assistance conditions changed, exhibiting a local maximum at approximately 30% of sit-to-stand. The *Above* alignment condition exhibited the largest local maxima displacement. The *Below* alignment condition showed the most change from beginning to the end of sit-to-stand. The prismatic pDOF showed a systematic change in displacement as well, decreasing with increasing assistance level, and also changing shape around 30% of sit-to-stand. The *Above* alignment condition exhibited the largest local minimum and the smallest range of displacement from beginning to end of sit-to-stand. The *Below* alignment condition showed the most change from beginning to the end of sit-to-stand.

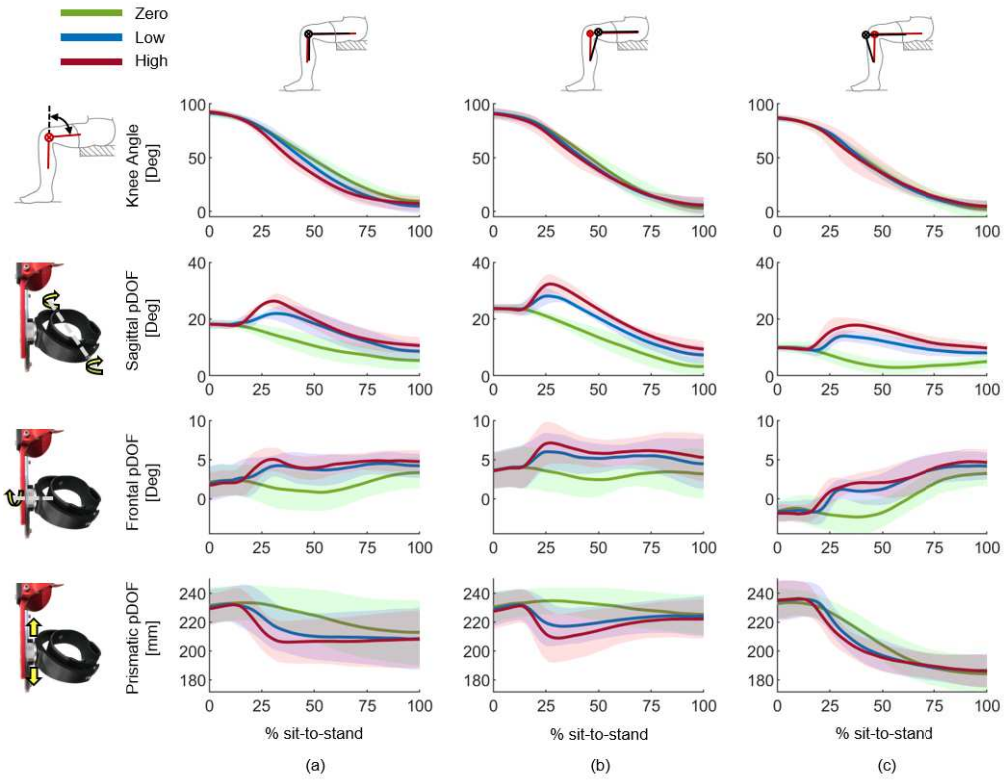

Fig. 12. Mean values (solid lines) and standard deviations (shaded areas) of the knee joint angle and the pDOFs displacements measured during the sit-to-stand transitions. Ideal alignment case is shown in (a), Above case is shown in (b), and Below case is shown in (c). The assistance levels are indicated with different colors. The prismatic pDOF plot shows the absolute position relative to the exoskeleton's point of rotation. Sagittal pDOF and frontal pDOF plots show the relative angle between the exoskeleton shank segment and the human shank in sagittal and frontal planes respectively. The assistance levels are indicated with different colors: zero assistance in green, low assistance in blue, and high assistance in red.

V. Discussion

A. Human Experiments

Misalignments between an exoskeleton and the user's joint may result in undesired spurious forces and torques [10]. Theoretically, misalignments can be due to (1) inaccuracy in locating the anatomical joint axis when the exoskeleton is donned by the user, (2) sliding of the exoskeleton with respect to the user's limb after the exoskeleton is donned, (3) soft tissue deformations due to the physical interaction between the exoskeleton and the user's limb, and (4) physiological movements of the anatomical joint within the range of motion [29]. In addition, if the exoskeleton is designed to using a pure rotary joint, it is intrinsically incompatible with human knee joint due to non-constant location of the anatomical joint axis. Motion capture is necessary to assess misalignments in powered exoskeletons.

Our motion capture analysis shows that the exoskeleton knee axis is misaligned with the anatomical knee axis even in the *Ideal* alignment condition (Fig. 9). In addition, the analysis of misalignment in the *Above* and *Below* conditions (Fig. 9(b-c)) shows that the alignment conditions affect the path of the exoskeleton knee axis relative to the human knee axis during sit-to-stand transitions. In agreement with previous modeling studies [13], the misalignment is not constant (Fig. 9), but changes as a function of the knee flexion/extension angle. In addition, our results show that the misalignment is affected by the assistive torque applied by the exoskeleton (see markers with different colors in Fig. 9). Our results also show that both *Low* and *High* assistive torques result in larger displacements of the exoskeleton knee axis compared to the *Zero* assistance condition (i.e., transparent mode). Interestingly, the assistive torque may result in a temporary reduction of the misalignment, depending on the location of the exoskeleton and the level of assistance (for example, Fig. 9 (c), *High*). These observations seem to generalize well across different subjects (Fig. 9). Cumulatively, these results show that misalignment between the exoskeleton and user knee joint is unavoidable and depends on the exoskeleton assistance, the initial alignment, and the torque provided by the exoskeleton, but that the effect of these variables on misalignment is quite consistent across subjects.

Modeling studies show that pDOFs have the potential to dynamically compensate for misalignments [13]. For this compensation to work in a physical system, the pDOFs must be able to move freely (i.e., negligible friction) while sustaining the load due to the assistive torque generated by the exoskeleton. We found that the range of motion of the pDOFs in the Utah ExoKnee was not impacted by alignment or assistance condition (Fig. 12). This result suggests that friction in the pDOF was negligible. On the other hand, we found that the path of movement of all pDOFs was impacted by the assistance level, particularly around 30% of sit-to-stand,

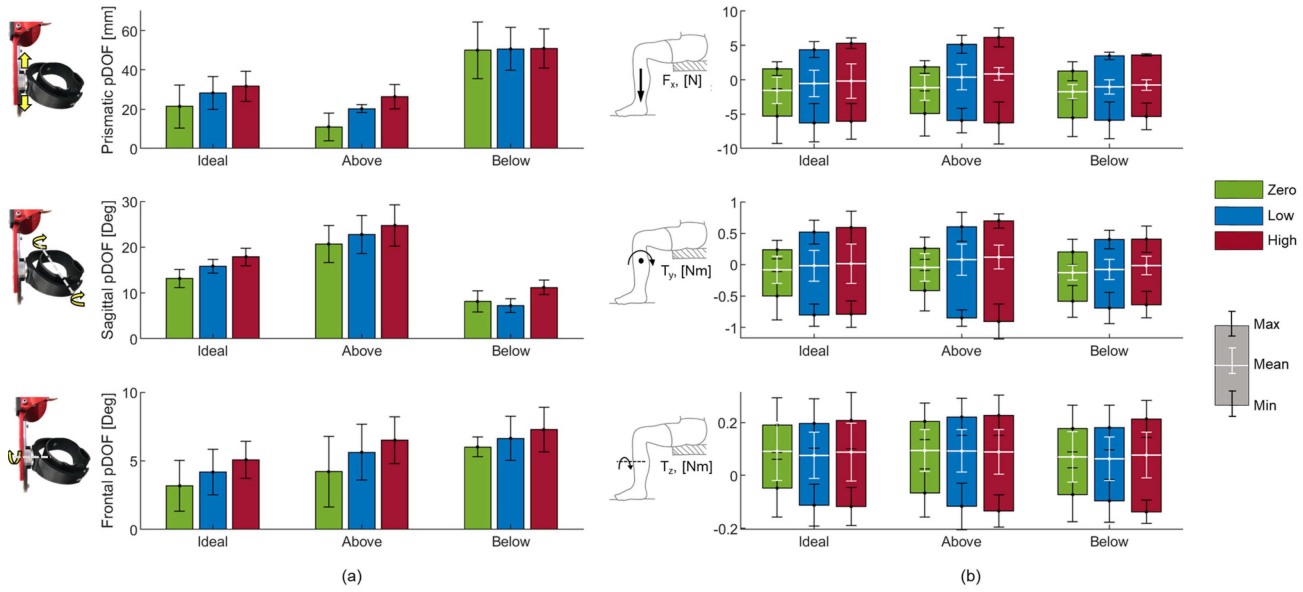

Fig. 13. Ranges of movement (mean ± std) for each pDOF are shown in panel (a). The values of the maximum (mean ± std), minimum (mean ± std), and mean (mean ± std) force are shown in (b). Each one of these values was averaged across all subjects and trials. The white line with error bars shows the mean value of the force, the top and bottom edges of the rectangles in (b) represent the maximum and minimum values of the forces respectively. The assistance levels are indicated with different colors: zero assistance in green, low assistance in blue, and high assistance in red.

when the peak assistive torque was applied (Fig. 12). This result is coherent with the observed effect of the assistance on the misalignment (Fig. 9). Overall, our results show that the pDOFs dynamically align the exoskeleton and user joint axes, even when the exoskeleton is providing a large assistive torque.

The goal of the pDOFs is to prevent the spurious forces and torques on the user's limb that can result from misalignments. We hypothesized that, in the proposed self-aligning exoskeleton, misalignments between the user and the exoskeleton joint axes will not result in an increase of spurious forces and torques on the user. To test this hypothesis, we have measured the interaction forces between the exoskeleton and the user across different alignment and assistance conditions. The analysis of the interaction forces (Fig. 11 and IV-B) shows that the spurious forces (F_x and F_y) and torques (T_x, T_y, T_z) were not visibly affected by the assistance level. On the other hand, F_z increased with the level of assistance. This result is not surprising given that F_z is roughly perpendicular to the user shank, and, therefore, it is not a spurious load. Relatively large standard deviations were observed in measured interaction forces (Fig. 11). The large standard deviation in F_z is likely due to inter-subject variability in sit-to-stand timing as our controller allows the subjects to stand up at their preferred speed. The standard deviations in all other forces and torques, are large relative to the value of the mean because the measured values themselves are small. The linear regression analysis showed that no forces or torques other than F_z were significantly correlated to the assistive joint torque. The measured peaks of the spurious forces and torques were 5 N and 0.5 Nm, respectively (Fig. 11). To put these numbers in perspective, a previous study [11] testing similar misalignment conditions using a powered exoskeleton with no self-aligning mechanism showed spurious forces and torques up to 50 N and 10 Nm, respectively. Thus, the analysis of the interaction forces and torques supports our hypothesis.

B. Design and Control

The pDOFs in a self-aligning mechanism should be designed to work smoothly under the high load generated by the actuation system during assistance. The pDOFs should also be lightweight and unobtrusive, as adding significant weight or dimension to the exoskeleton may negate its assistive function [30]. The proposed design includes two pDOFs in the Sagittal plane to compensate for vertical misalignments of the powered axis. Our design also includes one pDOF in the frontal plane to accommodate for physiological variations in the knee varus/valgus angle, allowing the exoskeleton to be used on both right and left legs and by different users, without hardware modifications (Fig. 1). As a result of the proposed symmetric design (Fig. 1) of our knee exoskeleton, the reaction forces acting on the self-aligning mechanism during assistance are naturally balanced and no torsion is generated, so the pDOFs can be made lightweight. The self-aligning mechanism accounts for only 5.3% (0.190 kg) of total exoskeleton weight (3.6 kg) and all pDOFs are integrated within the exoskeleton frame. Thus, in the proposed design, the pDOFs can transmit high assistive torques, while having a minimal effect on the weight and dimensions of the powered exoskeleton.

In this paper, we propose a novel approach to control sit-to-stand transitions with a powered knee exoskeleton. Assistive strategies developed for individuals with spinal cord injury rely on stiff closed-loop position controllers that enforce a specified sit-to-stand trajectory without requiring active participation of the user [31]. In contrast, systems developed for healthy subjects rely on closed-loop torque control with no predefined

position trajectory [32]. For example, in [33] a gaussian curve with fixed centroid and variable torque peak is used to determine the assistive torque provided by the exoskeleton, whereas electromyography is used in [34]. In our controller, the assistive torque trajectory is adapted at the beginning of the sit-to-stand movement by determining the location of the peak torque, normalized by the knee angle when the user is sitting (Fig. 5, Fig. 10). This adaptive strategy has the potential to make the assistive controller more robust to variations in user anthropometry and seat height.

The Utah ExoKnee uses a PID controller with a DOB after [35]. Bench top testing (Fig. 5) show that the performance of the proposed torque controller (i.e., 22.3 Hz -3dB bandwidth) should be sufficient to assist common activities of daily living based on the data in [36], [37]. However, in this paper, we only focused on sit-to-stand transitions, which require high torque and low speed (Fig. 4). Additional experiments should be performed to validate the performance of the torque controller on ambulation activities that require low torque and high speed, such as walking.

C. Limitations

The interaction torque in the X-axis (T_x, parallel to the user's shank) was not compensated for by a pDOF. Given the symmetric design of the proposed exoskeleton, it should be possible to add a rotational pDOF in the X-axis while still being able to transfer assistive torque in the sagittal plane. This pDOF could be implemented, for example, using a custom curvilinear guide as done in [12], [38]. Further studies are necessary to investigate the viability and effect of adding this additional pDOF.

For the purpose of this study, the peak torque during sit-to-stand transitions was regulated by the experimenter. However, customization of assistance level to the user needs is necessary. Future work should investigate scaling the assistance levels by body weight or level of impairment. In addition, in our experiments, the sit-to-stand mode was activated by the experimenter. Although the subject could decide when to stand up, and the sit-to-stand transitions could be performed at subjects self-selected speed, it would be valuable to automatically detect the user's intention to transition into the sit-to-stand mode, as previously done in powered prostheses [39].

We show that the interaction forces do not change as a function of the alignment or the assistive torque, which validates the proposed lightweight self-aligning mechanism. However, it is not clear what would happen without pDOF. A previous study suggests that the interaction forces would increase significantly [11], but it is unclear if the observed increase in the interaction forces/torques influences the users' comfort. In agreement with the interaction force/torque measurement result, participants in our study did not report differences in comfort between the three alignment conditions. However, further studies are necessary to investigate users' comfort, which has been previously done only with an upper limb exoskeleton [40].

VI. Conclusion

Self-aligning mechanisms for powered exoskeletons aim to address the need for comfortable and safe human-robot interaction. Previous studies have investigated self-aligning mechanisms using analytical models, simulations, and physical prototypes. This paper presents the first experimental validation using direct measurements of interaction forces and torques at the human-robot interface with controlled misalignments introduced by the experimenter. Four healthy subjects performed sit-to-stand transitions with the proposed knee exoskeleton with varying alignment and assistance conditions. This experiment showed that the spurious interaction forces and torques are not affected by the level of assistance or the alignment condition. Additionally, the passive degrees of freedom successfully compensate for variations in the exoskeleton alignment observed for different knee joint positions and assistance levels. Cumulatively, our results show that the proposed self-aligning mechanism can effectively compensate for misalignments during assistive tasks that require high assistive torque such as sit-to-stand transitions. Further studies are necessary to assess if the proposed self-aligning mechanism affects the user's perceived effort level and comfort, as done in [40].

References

[1] M. A. Ergin and V. Patoglu, "A self-adjusting knee exoskeleton for robot-assisted treatment of knee injuries," *IEEE Int. Conf. Intell. Robot. Syst.*, pp. 4917–4922, 2011.

[2] L. M. Mooney, E. J. Rouse, and H. M. Herr, "Autonomous exoskeleton reduces metabolic cost of human walking while carrying a load," *J. Neuroeng. Rehabil.*, 2014.

[3] T. Lenzi, D. Zanotto, P. Stegall, M. C. Carrozza, and S. K. Agrawal, "Reducing muscle effort in walking through powered exoskeletons," *Proc. Annu. Int. Conf. IEEE Eng. Med. Biol. Soc. EMBS*, pp. 3926–3929, 2012.

[4] S. Lefmann, R. Russo, and S. Hillier, "The effectiveness of robotic-assisted gait training for paediatric gait disorders: Systematic review," *J. Neuroeng. Rehabil.*, vol. 14, no. 1, pp. 1–10, 2017.

[5] L. Saccares, I. Sarakoglou, and N. G. Tsagarakis, "It-knee: An exoskeleton with ideal torque transmission interface for ergonomic power augmentation," *IEEE Int. Conf. Intell. Robot. Syst.*, vol. 2016-Novem, pp. 780–786, 2016.

[6] H. Kazerooni, "Exoskeletons for Human Power Augmentation."

[7] S. Kim, M. A. Nussbaum, M. I. Mokhlespour Esfahani, M. M. Alemi, S. Alabdulkarim, and E. Rashedi, "Assessing the influence of a passive, upper extremity exoskeletal vest for tasks requiring arm elevation: Part I – 'Expected' effects on discomfort, shoulder muscle activity, and work task performance," *Appl. Ergon.*, vol. 70, no. September 2017, pp. 315–322, 2018.

[8] N. Jarrassé and G. Morel, "Connecting a human limb to an exoskeleton," *IEEE Trans. Robot.*, vol. 28, no. 3, pp. 697–709, 2012.

[9] M. A. Lafortune, "Three-Dimensional Kinematics of the Human Knee During Walking," *J. Biomech.*, vol. 25, no. 4, pp. 347–357, 1992.

[10] D. Wang, K. M. Lee, J. Guo, and C. J. Yang, "Adaptive knee joint exoskeleton based on biological geometries," *IEEE/ASME Trans. Mechatronics*, vol. 19, no. 4, pp. 1268–1278, 2014.

[11] D. Zanotto, Y. Akiyama, P. Stegall, and S. K. Agrawal, "Knee Joint Misalignment in Exoskeletons for the Lower Extremities: Effects on User's Gait," *IEEE Trans. Robot.*, vol. 31, no. 4, pp. 978–987, 2015.

[12] A. H. A. Stienen, E. E. G. Hekman, F. C. T. van der Helm, and H. van der Kooij, "Self-aligning exoskeleton axes through decoupling of joint rotations and translations," *IEEE Trans. Robot.*, vol. 25, no. 3, pp. 628–633, 2009.

[13] M. Cempini, S. M. M. De Rossi, T. Lenzi, N. Vitiello, and M. C. Carrozza, "Self-alignment mechanisms for assistive wearable robots: A kinetostatic compatibility method," *IEEE Trans. Robot.*, vol. 29, no. 1, pp. 236–250, 2013.

[14] V. A. D. Cai, P. Bidaud, V. Hayward, F. Gosselin, and E. Desailly, "Self-adjusting, Isostatic Exoskeleton for The Human Knee Joint," *2011 Annu. Int. Conf. Ieee Eng. Med. Biol. Soc.*, pp. 612–618, 2011.

[15] B. Celebi, M. Yalcin, and V. Patoglu, "AssistOn-Knee: A self-aligning knee exoskeleton," *IEEE Int. Conf. Intell. Robot. Syst.*, pp. 996–1002, 2013.

[16] K. Junius, M. Degelaen, N. Lefeber, E. Swinnen, B. Vanderborght, and D. Lefeber, "Bilateral, Misalignment- Compensating, Full- DOF Hip Exoskeleton?: Design and Kinematic Validation," *Appl. Bionics Biomech.*, vol. 2017, 2017.

[17] K. Junius, N. Lefeber, E. Swinnen, B. Vanderborght, and D. Lefeber, "Metabolic effects induced by a kinematically compatible hip exoskeleton during STS," *IEEE Trans. Biomed. Eng.*, vol. 65, no. 6, pp. 1399–1409, 2017.

[18] F. Giovacchini *et al.*, "A light-weight active orthosis for hip movement assistance," *Rob. Auton. Syst.*, vol. 73, pp. 123–134, 2015.

[19] J. H. Kim *et al.*, "Design of a Knee Exoskeleton Using Foot Pressure and Knee Torque Sensors," *Int. J. Adv. Robot. Syst.*, vol. 12, no. 8, 2015.

[20] D. J. Hyun, H. Park, T. Ha, S. Park, and K. Jung, "Biomechanical design of an agile, electricity-powered lower-limb exoskeleton for weight-bearing assistance," *Rob. Auton. Syst.*, vol. 95, pp. 181–195, 2017.

[21] J. Wang *et al.*, "Comfort-Centered Design of a Lightweight and Backdrivable Knee Exoskeleton," *IEEE Robot. Autom. Lett.*, vol. 3, no. 4, pp. 4265–4272, 2018.

[22] D. A. Winter, *The Biomechanics and Motor Control of Human Gait*, 2nd ed. Waterloo, Ontario, Canada: University of Waterloo Press, 1991.

[23] T. Lenzi, M. Cempini, L. Hargrove, and T. Kuiken, "Design, development, and testing of a lightweight hybrid robotic knee prosthesis," *Int. J. Rob. Res.*, vol. 37, no. 8, pp. 953–976, Jul. 2018.

[24] N. Paine, S. Oh, and L. Sentis, "Design and control considerations for high-performance series elastic actuators," *IEEE/ASME Trans. Mechatronics*, vol. 19, no. 3, pp. 1080–1091, 2014.

[25] S. Oh and K. Kong, "High-Precision Robust Force Control of a Series Elastic Actuator," *IEEE/ASME Trans. Mechatronics*, vol. 22, no. 1, pp. 71–80, 2017.

[26] M. Tran, L. Gabert, M. Cempini, and T. Lenzi, "A Lightweight, Efficient Fully Powered Knee Prosthesis with Actively Variable Transmission," *IEEE Robot. Autom. Lett.*, vol. 4, no. 2, pp. 1186–1193, 2019.

[27] T. Lenzi, M. C. Carrozza, and S. K. Agrawal, "Powered hip exoskeletons can reduce the user's hip and ankle muscle activations during walking," *IEEE Trans. Neural Syst. Rehabil. Eng.*, vol. 21, no. 6, pp. 938–948, 2013.

[28] R. M. Ehrig, W. R. Taylor, G. N. Duda, and M. O. Heller, "A survey of formal methods for determining functional joint axes," *J. Biomech.*, 2007.

[29] M. B. Näf, K. Junius, M. Rossini, C. Rodriguez-Guerrero, B. Vanderborght, and D. Lefeber, "Misalignment Compensation for Full Human-Exoskeleton Kinematic Compatibility: State of the Art and Evaluation," *Appl. Mech. Rev.*, vol. 70, no. 5, p. 050802, 2019.

[30] L. M. Mooney, E. J. Rouse, and H. M. Herr, "Autonomous exoskeleton reduces metabolic cost of human walking during load carriage," *J. Neuroeng. Rehabil.*, vol. 11, 2014.

[31] J. L. Contreras-Vidal *et al.*, "Powered exoskeletons for bipedal locomotion after spinal cord injury," *Journal of Neural Engineering*. 2016.

[32] T. Yan, M. Cempini, C. M. Oddo, and N. Vitiello, "Review of assistive strategies in powered lower-limb orthoses and exoskeletons," *Rob. Auton. Syst.*, vol. 64, pp. 120–136, 2015.

[33] M. K. Shepherd and E. J. Rouse, "Design and Validation of a Torque-Controllable Knee Exoskeleton for Sit-to-Stand Assistance," *IEEE/ASME Trans. Mechatronics*, vol. 22, no. 4, pp. 1695–1704, 2017.

[34] M. Lyu, W.-H. Chen, X. Ding, J. Wang, Z. Pei, and B. Zhang, "Development of an EMG-Controlled Knee Exoskeleton to Assist Home Rehabilitation in a Game Context," *Front. Neurorobot.*, 2019.

[35] N. Paine, S. Oh, and L. Sentis, "Design and Control Considerations for High Performance Series Elastic Actuators," *IEEE/ASME Trans. Mechatronics*, vol. PP, no. 99, pp. 1–12, 2013.

[36] D. a Winter, "Energy generation and absorption at the ankle and knee during fast, natural, and slow cadences.," *Clin. Orthop. Relat. Res.*, no. 175, pp. 147–54, May 1983.

[37] R. Riener, M. Rabuffetti, and C. Frigo, "Stair ascent and descent at different inclinations.," *Gait Posture*, vol. 15, no. 1, pp. 32–44, Feb. 2002.

[38] N. Vitiello *et al.*, "NEUROExos: A powered elbow exoskeleton for physical rehabilitation," *IEEE Trans. Robot.*, vol. 29, no. 1, pp. 220–235, 2013.

[39] H. A. Varol, F. Sup, and M. Goldfarb, "Multiclass real-time intent recognition of a powered lower limb prosthesis.," *IEEE Trans. Biomed. Eng.*, vol. 57, no. 3, pp. 542–51, Mar. 2010.

[40] A. Schiele, "Ergonomics of exoskeletons: Subjective performance metrics," *2009 IEEE/RSJ Int. Conf. Intell. Robot. Syst. IROS 2009*, pp. 480–485, 2009.